

A bright γ -ray flare interpreted as a giant magnetar flare in NGC 253


<https://doi.org/10.1038/s41586-020-03076-9>

Received: 17 August 2020

Accepted: 2 November 2020

Published online: 13 January 2021

 Check for updates

D. Svinkin¹, D. Frederiks¹, K. Hurley², R. Aptekar¹, S. Golenetskii¹, A. Lysenko¹, A. V. Ridnaia¹, A. Tsvetkova¹, M. Ulanov¹, T. L. Cline³, I. Mitrofanov⁴, D. Golovin⁴, A. Kozyrev⁴, M. Litvak⁴, A. Sanin⁴, A. Goldstein⁵, M. S. Briggs⁶, C. Wilson-Hodge⁷, A. von Kienlin⁸, X.-L. Zhang⁹, A. Rau⁹, V. Savchenko⁹, E. Bozzo⁹, C. Ferrigno⁹, P. Ubertini¹⁰, A. Bazzano¹⁰, J. C. Rodi¹⁰, S. Barthelmy³, J. Cummings¹¹, H. Krimm¹², D. M. Palmer¹³, W. Boynton¹⁴, C. W. Fellows¹⁴, K. P. Harshman¹⁴, H. Enos¹⁴ & R. Starr¹⁵

Soft γ -ray repeaters exhibit bursting emission in hard X-rays and soft γ -rays. During the active phase, they emit random short (milliseconds to several seconds long), hard-X-ray bursts, with peak luminosities¹ of 10^{36} to 10^{43} erg per second. Occasionally, a giant flare with an energy of around 10^{44} to 10^{46} erg is emitted². These phenomena are thought to arise from neutron stars with extremely high magnetic fields (10^{14} to 10^{15} gauss), called magnetars^{1,3,4}. A portion of the second-long initial pulse of a giant flare in some respects mimics short γ -ray bursts^{5,6}, which have recently been identified as resulting from the merger of two neutron stars accompanied by gravitational-wave emission⁷. Two γ -ray bursts, GRB 051103 and GRB 070201, have been associated with giant flares^{2,8–11}. Here we report observations of the γ -ray burst GRB 200415A, which we localized to a 20-square-arcmin region of the starburst galaxy NGC 253, located about 3.5 million parsecs away. The burst had a sharp, millisecond-scale hard spectrum in the initial pulse, which was followed by steady fading and softening over 0.2 seconds. The energy released (roughly 1.3×10^{46} erg) is similar to that of the superflare^{5,12,13} from the Galactic soft γ -ray repeater SGR 1806–20 (roughly 2.3×10^{46} erg). We argue that GRB 200415A is a giant flare from a magnetar in NGC 253.

On 15 April 2020, the extremely bright, short γ -ray burst GRB 200415A occurred at 08:48:06 UTC at Earth, and was detected by five space-based missions of the Interplanetary Network of γ -ray detectors (IPN, Methods). Here we report the final localization of the burst by the IPN to a roughly 20-arcmin² region (Methods) that overlaps with the central part of the nearby galaxy NGC 253, at a distance of $D_{\text{NGC253}} \approx 3.5$ Mpc (ref.¹⁴) (Fig. 1). The chance occurrence for GRB 200415A to be spatially consistent with a nearby galaxy likely to produce detectable giant flares is approximately 1 in 200,000 (ref.¹⁵).

GRB 200415A triggered Konus–Wind at $T_0 = 08:48:01.403$ UTC. As observed by Konus–Wind, the lightcurve of the burst starts with the fast (around 2 ms) rise of a narrow (around 4 ms) initial spike, which is followed by an exponentially decaying phase with a count-rate e-folding time of $\tau_{\text{cr}} \approx 50$ ms (Fig. 2a). The total duration of the burst is 0.138 s, and T_{90} (the duration of the time interval that contains the central 90% of the total count fluence of the burst) is 0.100 ± 0.014 s (hereafter, all the quoted uncertainties are at the 68% confidence level).

The hardness of the burst (the ratio between the 390–1,600-keV and 90–390-keV count rates) increases rapidly during the initial spike, peaks during the following approximately 8 ms and then decays gradually

with the count rate of the burst. Our spectral analysis (Methods) shows that, starting from the rise of the spike and up to about $T_0 + 100$ ms, the energy spectrum of the burst is well described by a cutoff power-law function (proportional to $E^\alpha \exp[-E(\alpha + 2)/E_p]$). The temporal evolution of the spectrum is illustrated in Fig. 2, which shows the behaviour of the cutoff power-law model parameters: the peak energy E_p , which corresponds to the maximum of the spectral energy distribution νF_ν , where F_ν is the energy flux per unit frequency interval at frequency ν (Fig. 2b) and the photon power-law index α (Fig. 2d). The initial spike is characterized by $E_p \approx 1.2$ MeV, with $\alpha \approx -0.6$. This E_p was the highest reached in the entire event. A non-thermal cutoff power-law model, with E_p decaying nearly exponentially, adequately describes burst spectra up to about $T_0 + 100$ ms. Afterwards, the very hard photon index α becomes poorly constrained; and, simultaneously, the emission spectrum can be described by a blackbody function (with a temperature $kT \approx 70$ keV), which is excluded by our analysis at the initial stage of the burst.

In Fig. 2c we show the temporal evolution of the 20 keV–10 MeV energy flux. It peaks in the initial spike with a 4-ms peak flux of $0.96_{-0.16}^{+0.32} \times 10^{-3}$ erg cm⁻² s⁻¹ and, starting from around $T_0 + 50$ ms, decays with $\tau_{\text{flux}} \approx 30$ ms. The time-integrated spectrum, measured

¹Ioffe Institute, St Petersburg, Russia. ²Space Sciences Laboratory, University of California, Berkeley, CA, USA. ³NASA Goddard Space Flight Center, Greenbelt, Maryland, USA. ⁴Space Research Institute, Moscow, Russia. ⁵Science and Technology Institute, Universities Space Research Association, Huntsville, AL, USA. ⁶Space Science Department, University of Alabama in Huntsville, Huntsville, AL, USA. ⁷NASA Marshall Space Flight Center, Huntsville, AL, USA. ⁸Max-Planck-Institut für extraterrestrische Physik, Garching, Germany. ⁹Department of Astronomy, University of Geneva, Versoix, Switzerland. ¹⁰INAF – Institute for Space Astrophysics and Planetology, Roma, Italy. ¹¹Center for Astrophysical Sciences, Johns Hopkins University, Baltimore, MD, USA.

¹²National Science Foundation, Alexandria, VA, USA. ¹³Los Alamos National Laboratory, Los Alamos, NM, USA. ¹⁴Lunar and Planetary Laboratory, University of Arizona, Tucson, AZ, USA.

¹⁵Catholic University of America, Washington, DC, USA. ✉e-mail: svinkin@mail.ioffe.ru

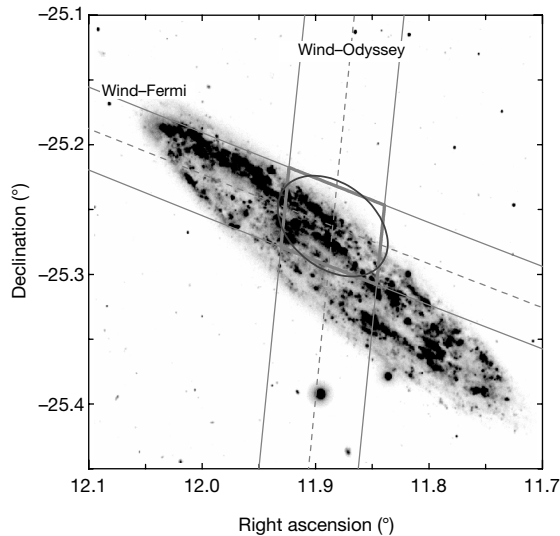


Fig. 1 | The final IPN localization of GRB 200415A. The localization is superimposed on an image of the NGC 253 galaxy from the GALEX survey (1,750–2,800 Å; Methods). It is defined by the 4.73-arcmin-wide Wind (Konus)–Odyssey (HEND) and 3.58-arcmin-wide Wind (Konus)–Fermi (GBM) annuli. The IPN error box (grey parallelogram) is shown along with the 20 arcmin² 3σ error ellipse for the position. The coordinates are J2000.

from T_0 to $T_0 + 0.192$ s, is best described by a sum of non-thermal (cutoff power-law) and thermal (blackbody) components (see Extended Data Table 1 for the model parameters). The total burst fluence is $8.5_{-1.0}^{+1.2} \times 10^{-6}$ erg cm⁻² in the 20 keV–10 MeV band.

A preliminary analysis of the Konus–Wind detection¹⁶ of GRB 200415A revealed its remarkable similarity to GRB 051103, historically the first extragalactic giant-flare candidate outside the Local Group, associated with the M81/M82 group of galaxies^{8–10} at a distance of $D_{\text{M81/M82}} \approx 3.6$ Mpc (ref. ¹⁷). To explore this similarity further, we performed a detailed comparison between the temporal and spectral properties of GRB 200415A and GRB 051103. The bursts have similar lightcurve and spectral evolution patterns (Fig. 2; Extended Data Tables 1, 5, 6). Although the peak count rates, reached in the first 2 ms of the initial spikes, are very similar (about $(1.5\text{--}1.7) \times 10^5$ s⁻¹), the photon flux over the entire extent of the decaying phase is about twice as high in GRB 051103 as in GRB 200415A. The initial pulses of both bursts are best described by the cutoff power-law model, with $E_p \approx 1.2$ MeV, but GRB 051103 has a much harder $\alpha \approx -0.1$. In contrast to GRB 200415A, the hardest emission in GRB 051103 ($E_p \approx 3$ MeV, $\alpha \approx 0.2$) was observed during the roughly 30 ms immediately after the initial spike. In accordance with the similarities of the bursts in peak count rate and E_p , measured in the initial spikes, their 4-ms peak flux estimates also agree within uncertainties. The blackbody components in the time-integrated spectra of GRB 200415A and GRB 051103 have similar temperatures ($kT \approx 100$ keV), with blackbody contributions to the total fluence of about 14% and 9%, respectively. The contribution of the initial short spike to the total fluence is about 45% for GRB 200415A and 13% for GRB 051103.

Thus, the extremely bright, short GRB 200415A, which strong evidence suggests is associated with the NGC 253 galaxy, is remarkably similar to GRB 051103, which presumably originated from the M81/M82 group of galaxies at nearly the same distance, in terms of light curve morphology, spectral behaviour and observed peak energy flux. A lightcurve with a bright, millisecond-scale initial pulse followed by an exponentially decaying emission is unusual for short cosmological γ -ray bursts (GRBs); none of more than about 500 short bursts detected by Konus–Wind in more than 25 years of observations displays such a shape^{15,18}. On the other hand, this pattern was observed in two Galactic giant flares, from SGR 1900+14^{19,20} and SGR 1806–20^{20,21}.

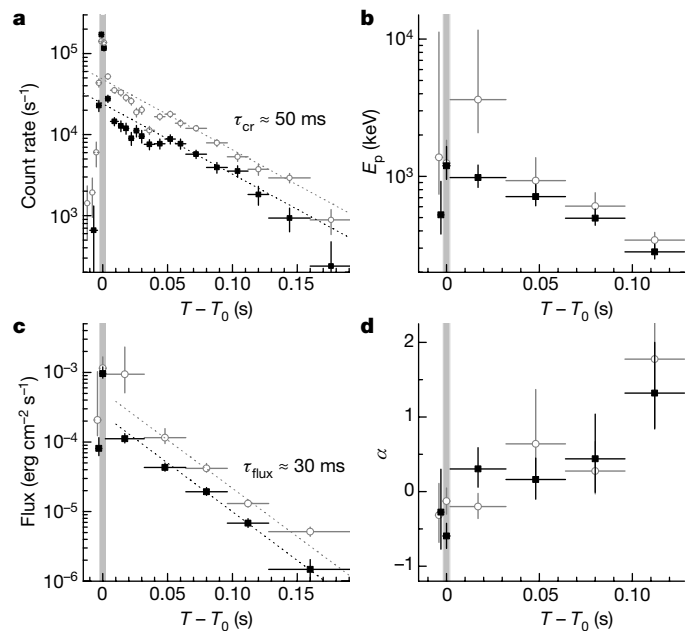


Fig. 2 | Time histories of GRB 051103 (open symbols) and GRB 200415A (filled symbols) and evolution of their spectral parameters. All times are given relative to the Konus–Wind trigger time T_0 . **a**, Burst time histories as recorded by Konus–Wind. Both events start with a sharp rise of an exceptionally bright, narrow (4 ms) initial spike (grey shaded area), followed by an exponential decay with $\tau_{\text{cr}} \approx 50$ ms (dotted lines). **b, d**, The temporal evolution of the emission spectra is illustrated by the behaviour of the best-fitting parameters of the cutoff power-law model: the peak energy E_p (**b**) and the photon power-law index α (**d**). Both bursts are characterized by $E_p \approx 1.2$ MeV in the initial pulse, which is the hardest part of GRB 200415A, whereas the hardest emission in GRB 051103 (with $E_p \approx 3$ MeV) was detected during the subsequent approximately 30 ms. A non-thermal cutoff power-law model adequately describes burst spectra up to about $T_0 + 100$ ms; afterwards, the hard power-law photon index α becomes poorly constrained and, simultaneously, the emission spectrum can be described by a blackbody function with $kT \approx 70\text{--}100$ keV. **c**, Evolution of the 20 keV–10 MeV energy flux, which, in both cases, peaks in the initial spike (grey shaded area) and, starting from about $T_0 + 50$ ms, decays with $\tau_{\text{flux}} \approx 30$ ms (dotted lines). Vertical error bars indicate 68% confidence intervals; horizontal error bars indicate the duration of the interval.

Furthermore, higher-time-resolution lightcurves of GRB 200415A from Swift–Burst Alert Telescope (BAT) and Fermi–Gamma-ray Burst Monitor (GBM)²² have an initial short (less than 1 ms) subpeak, followed by a sharp decrease for approximately 1 ms, before the main part of the peak. This pattern is also seen in SGR 1806–20¹² and may be a general property of giant flares that can be used to identify them within the short-GRB sample. Thus, the interpretation of GRB 200415A and GRB 051103 as magnetar giant flares is strongly suggested, with additional support provided by the non-detection of an accompanying gravitational-wave signal for GRB 051103²³ (there is no sensitive coverage by a gravitational-wave detector for GRB 200415A).

At source distances of $D_{\text{NGC253}} = 3.5$ Mpc and $D_{\text{M81}} = 3.6$ Mpc, the characteristic radius of the emission region, estimated from the blackbody spectral fits, is $R \approx 20\text{--}40$ km, the same order of magnitude as the radius of a neutron star or its magnetosphere. The implied isotropic-equivalent energy release in γ -rays for GRB 200415A (GRB 051103) is $E_{\text{iso}} \approx 1.3 \times 10^{46}$ erg ($E_{\text{iso}} \approx 5.3 \times 10^{46}$ erg) and the isotropic-equivalent peak luminosity is $L_{\text{iso}} \approx 1.4 \times 10^{48}$ erg s⁻¹ ($L_{\text{iso}} \approx 1.8 \times 10^{48}$ erg s⁻¹). Therefore, the total energies released in both flares are comparable with that estimated for the most energetic flare from a Galactic magnetar^{5,12,13}. Taken together, these results make GRB 200415A and GRB 051103 the most

substantial candidates for extragalactic magnetar giant flares: both are at least about five times more luminous than any Galactic magnetar flare observed previously². Such high luminosities may indicate that the magnetar sources of GRB 200415A and GRB 051103 are younger than a few hundred years, so their magnetic fields are strong enough to power such flares^{5,24}. Assuming the same spectra and energetics, similar events could be detected with Konus–Wind from distances up to around 16 Mpc.

Despite the strong evidence in favour of the giant-flare nature of GRB 200415A and GRB 051103, it cannot completely be ruled out that they might belong to an as-yet-undiscovered branch of the cosmological short-GRB population. For the observed energy fluence, and assuming a cosmological redshift of $z = 0.05\text{--}1$, GRB 200415A is consistent with the Konus–Wind sample of short GRBs with known redshifts^{25,26} in terms of a hardness–intensity relation in the cosmological rest frame (Extended Data Fig. 1). In the case of GRB 051103, the implied short-GRB redshift is $z \approx 1$, with intrinsic $E_p \approx 5$ MeV.

The detection of extragalactic giant flares facilitates the study of emission processes on millisecond and sub-millisecond timescales²²; such study is not possible for galactic events because they saturate almost all γ -ray detectors. On the timescale relevant to Konus–Wind (more than about 2 ms), the single-peaked GRB 200425A and GRB 051103 are clearly different from the third known extragalactic giant-flare candidate, GRB 070201², which has highly variable emission during the first roughly 50 ms. This suggests that the physical processes behind the emission in the initial pulses of giant flares may develop on timescales that span more than an order of magnitude.

The IPN box of GRB 200415A is projected partially into the nuclear region, the bar, a ring-like structure enclosing the bar and a spiral arm of NGC 253, which contain many young star groups²⁷. This is consistent with the Galactic magnetars, which are associated with the young stellar population²⁴. The current sample of giant-flare host galaxies includes five massive galaxies (the Milky Way, M31, M81/M82 group and NGC 253) and the Large Magellanic Cloud, which resemble the host galaxies of non-repeating fast radio bursts²⁸. This provides evidence for a connection between soft γ -ray repeaters and fast radio bursts.

Online content

Any methods, additional references, Nature Research reporting summaries, source data, extended data, supplementary information, acknowledgements, peer review information; details of author contributions and competing interests; and statements of data and code availability are available at <https://doi.org/10.1038/s41586-020-03076-9>.

1. Kaspi, V. M. & Beloborodov, A. M. Magnetars. *Annu. Rev. Astron. Astrophys.* **55**, 261–301 (2017).

2. Mazets, E. P. et al. A giant flare from a soft gamma repeater in the Andromeda galaxy (M31). *Astrophys. J.* **680**, 545–549 (2008).
3. Duncan, R. C. & Thompson, C. Formation of very strongly magnetized neutron stars: implications for gamma-ray bursts. *Astrophys. J.* **392**, L9–L13 (1992).
4. Mereghetti, S. et al. Magnetars: properties, origin and evolution. *Space Sci. Rev.* **191**, 315–338 (2015).
5. Hurley, K. et al. An exceptionally bright flare from SGR 1806–20 and the origins of short-duration γ -ray bursts. *Nature* **434**, 1098–1103 (2005).
6. Popov, S. B. & Stern, B. E. Soft gamma repeaters outside the Local Group. *Mon. Not. R. Astron. Soc.* **365**, 885–890 (2006).
7. Abbott, B. P. et al. Multi-messenger observations of a binary neutron star merger. *Astrophys. J.* **848**, L12 (2017).
8. Ofek, E. O. et al. The short-hard GRB 051103: observations and implications for its nature. *Astrophys. J.* **652**, 507–511 (2006).
9. Frederiks, D. D. et al. On the possibility of identifying the short hard burst GRB 051103 with a giant flare from a soft gamma repeater in the M81 group of galaxies. *Astron. Lett.* **33**, 19–24 (2007).
10. Hurley, K. et al. A new analysis of the short-duration, hard-spectrum GRB 051103, a possible extragalactic soft gamma repeater giant flare. *Mon. Not. R. Astron. Soc.* **403**, 342–352 (2010).
11. Ofek, E. O. et al. GRB 070201: a possible soft gamma-ray repeater in M31. *Astrophys. J.* **681**, 1464–1469 (2008).
12. Palmer, D. M. et al. A giant γ -ray flare from the magnetar SGR 1806–20. *Nature* **434**, 1107–1109 (2005).
13. Frederiks, D. D. et al. Giant flare in SGR 1806–20 and its Compton reflection from the Moon. *Astron. Lett.* **33**, 1–18 (2007).
14. Rekola, R. et al. Distance to NGC 253 based on the planetary nebula luminosity function. *Mon. Not. R. Astron. Soc.* **361**, 330–336 (2005).
15. Burns, E. et al. Identification of a local sample of gamma-ray bursts consistent with a magnetar giant flare origin. *Astrophys. J.* (in the press).
16. Frederiks, D. et al. Konus-Wind observation of GRB 200415A (a magnetar giant flare in Sculptor galaxy?). *GRB Coordinates Network* 27596 (2020).
17. Karachentsev, I. D. & Kashibadze, O. G. Masses of the local group and of the M81 group estimated from distortions in the local velocity field. *Astrophysics* **49**, 3–18 (2006).
18. Svinkin, D. S. et al. The second Konus-Wind catalog of short gamma-ray bursts. *Astrophys. J. Suppl. Ser.* **224**, 10 (2016).
19. Aptekar, R. L. et al. Konus Catalog of soft gamma repeater activity: 1978 to 2000. *Astrophys. J. Suppl. Ser.* **137**, 227–277 (2001).
20. Tanaka, Y. T. et al. Comparative study of the initial spikes of soft gamma-ray repeater giant flares in 1998 and 2004 observed with geotail: do magnetospheric instabilities trigger large-scale fracturing of a magnetar's crust? *Astrophys. J.* **665**, L55–L58 (2007).
21. Terasawa, T. et al. Repeated injections of energy in the first 600 ms of the giant flare of SGR 1806–20. *Nature* **434**, 1110–1111 (2005).
22. Roberts, O. J. et al. Rapid spectral variability of a giant flare from a magnetar in NGC 253. *Nature* <https://doi.org/10.1038/s41586-020-03077-8> (2021).
23. Abadie, J. et al. Implications for the origin of GRB 051103 from LIGO observations. *Astrophys. J.* **755**, 2 (2012).
24. Olausen, S. A. & Kaspi, V. M. The McGill magnetar catalog. *Astrophys. J. Suppl. Ser.* **212**, 6 (2014).
25. Tsvetkova, A. et al. The Konus-Wind catalog of gamma-ray bursts with known redshifts. I. Bursts detected in the triggered mode. *Astrophys. J.* **850**, 161 (2017).
26. Pozanenko, A. et al. GRB 200415A (possible magnetar giant flare in Sculptor galaxy): INTEGRAL observations. *GRB Coordinates Network* 27627 (2020).
27. Rodríguez, M. J. et al. Identification and analysis of the young population in the starburst galaxy NGC 253. *Mon. Not. R. Astron. Soc.* **479**, 961–972 (2018).
28. Heintz, K. E. et al. Host galaxy properties and offset distributions of fast radio bursts: implications for their progenitors. *Astrophys. J.* **903**, 152 (2020).

Publisher's note Springer Nature remains neutral with regard to jurisdictional claims in published maps and institutional affiliations.

© The Author(s), under exclusive licence to Springer Nature Limited 2021

Methods

Observations

GRB 200415A occurred at 08:48:06 UTC at Earth, and was detected by the GBM onboard the Fermi Gamma-ray Space Telescope Mission²⁹ and the BAT (outside the coded field of view) onboard the Neil Gehrels Swift Observatory³⁰ in low-Earth orbits; the SPI telescope anticoincidence system³¹ (SPI-ACS) and Pixellated Imaging Caesium Iodide Telescope^{32,33} (IBIS-PICsIT) instruments onboard the International Gamma-Ray Astrophysics Laboratory (INTEGRAL) in an eccentric Earth orbit 0.44 light seconds from Earth; the Mars–Odyssey High Energy Neutron Detector^{34,35} (HEND) in orbit around Mars 672 light seconds from Earth; the Konus–Wind³⁶ γ -ray spectrometer on the Wind mission³⁷ in a Lissajous orbit at the L_1 libration point of the Sun–Earth system at a distance of 4.8 light seconds; and the Modular X- and Gamma-Ray Sensor (MXGS) of The Atmosphere–Space Interactions Monitor ASIM³⁸ onboard the International Space Station (not a part of the IPN).

Two independent and consistent Fermi–GBM localizations^{39,40}, RoboBA⁴¹ and BALROG^{42,43}, were announced in GRB Coordinates Network circulars at 08:58 UTC and 09:11 UTC, respectively, each with a 3σ probability region covering more than 1,000 deg². By exploiting the difference in the arrival time of the γ -ray signals at the four IPN (see next section) instruments (GBM, BAT, HEND and SPI-ACS), a preliminary 1.5-deg² IPN error box was announced at 16:51 UTC⁴⁴, and it was pointed out that this event might be a magnetar giant flare in NGC 253 (the Sculptor galaxy) located at $D_{\text{NGC253}} \approx 3.5$ Mpc. The Fermi–LAT localization, announced at 19:30 UTC⁴⁵, was consistent with the box.

As soon as Konus–Wind data arrived, the improved 274-arcmin² box (about 20 times smaller than the initial box) was published, on 16 April 16:16 UTC⁴⁶, which strengthened the association of the burst with the galaxy. The box was close to the 68% confidence contours of the updated Fermi–LAT localization⁴⁷, published on 16 April 20:48 UTC, and inside the 2σ and 1σ contours of the GBM RoboBA and BALROG localizations, respectively. The IPN localization was within about 37° of the Sun, making X-ray and optical follow-up observations challenging. The only optical observation of NGC 253, which resulted in an upper limit, was reported by the MASTER telescope network on 17 April⁴⁸.

IPN. The IPN (<http://www.ssl.berkeley.edu/ipn3/>) is a group of spacecraft orbiting Earth and Mars equipped with GRB detectors used to localize GRBs⁴⁹. When a GRB arrives at two spacecraft, it may be localized (triangulated) to an annulus on the sky, determined by the measured propagation time delay and spacecraft positions. Three spacecraft produce two possible locations (IPN error boxes). The ambiguity can be eliminated by the addition of a fourth, non-coplanar spacecraft, by the anisotropic response of Konus–Wind or by the GBM localization⁵⁰.

The propagation time delay and its uncertainty are calculated by cross-correlation⁵¹. The systematic uncertainties are estimated using the comparison of IPN triangulations with precise GRB positions⁵⁰.

The declared onboard clock accuracy of the spacecraft are: down to 1 μ s for Fermi; about 200 μ s for Swift; less than about 1 ms for Wind; and about 100 μ s for INTEGRAL. For Mars–Odyssey, an overall 3σ systematic uncertainty, which includes timing and other effects derived from IPN observations of precisely localized GRBs, is better than 360 ms. The Wind clock drift information is provided at https://pwgdata.sci.gsfc.nasa.gov/pub/wind_clock/.

Near-Earth spacecraft ephemerides are derived from two-line elements available at <https://www.space-track.org> using the SGP8 model. The Wind predicted ephemerides and their description are available at https://spdf.gsfc.nasa.gov/pub/data/wind/orbit/pre_or and https://cdaweb.gsfc.nasa.gov/misc/NotesW.html#WI_OR_PRE, respectively. Mars–Odyssey ephemerides were taken from the Jet Propulsion Laboratory’s HORIZONS system (<https://ssd.jpl.nasa.gov/horizons.cgi>).

For the near-Earth spacecraft and Wind, ephemeris uncertainties contribute less than 1 ms to the propagation time delay, so we

conservatively assume a systematic error in Konus–GBM and Konus–BAT triangulations to be 1 ms. For the Konus–HEND and GBM–HEND triangulations, we take 360 ms as the 3σ systematic uncertainty.

For the GRB 200415A triangulation, we used the following lightcurves: 2-ms Konus (see Methods section ‘Konus–Wind’), 390–1,600 keV; 0.1-ms GBM, 360–1,000 keV, constructed from the time-tagged event data of triggered detectors (0, 1, 2, 3, 4, 5, 9 and a; only NaI data were used); 0.1-ms BAT, 25–350 keV, constructed from the time-tagged event data from the GUANO system⁵²; 250-ms HEND, 50–3,000 keV; and 7.8-ms INTEGRAL–PICsIT, 250–2,000 keV.

Using these data, we derived five annuli (Extended Data Table 2). The final IPN 3σ box was constructed from Konus–GBM and Konus–HEND annuli (Extended Data Table 3). We used the Konus–GBM annulus instead of the narrower Konus–BAT one owing to the similarity between the energy bands of the two instruments. GBM saturation occurred near the burst peak, but does not significantly affect the cross-correlation with the Konus 2-ms-resolution lightcurve.

The annuli were combined to yield an error ellipse⁵³ with a major axis corresponding to the Konus–GBM annulus and a minor axis corresponding to the Konus–HEND annulus. We obtain a 3σ error ellipse centred at a right ascension (J2000) of 11.885° and declination (J2000) of -25.263° , with major and minor axes of 6.25 arcmin and 4.07 arcmin, respectively, and a position angle of 61.135° . The area of the ellipse is 20 arcmin².

The ellipse contains the central part of NGC 253 (Fig. 1). The image was obtained with the Galaxy Evolution Explorer (GALEX)⁵⁴ during the GALEX Nearby Galaxies Survey⁵⁵ (observation ID, 2482083865531777024). The NGC 253 image was obtained via the MAST portal (<https://mast.stsci.edu>).

Konus–Wind

Konus–Wind³⁶ consists of two identical NaI(Tl) scintillation detectors, each with a 2π -sr field of view, mounted on opposite faces of the rotationally stabilized Wind spacecraft³⁷, such that one detector (S1) points towards the south ecliptic pole, thereby observing the south ecliptic hemisphere, while the other (S2) observes the north ecliptic hemisphere.

Each Konus–Wind detector is a cylinder 5 inches in diameter and 3 inches in height, placed into an aluminium container with a beryllium entrance window. The crystal scintillator is viewed by a photomultiplier tube through a 20-mm-thick lead glass, which provides effective detector shielding from the spacecraft’s background in the soft spectral range. The detector effective area is about 80–160 cm², depending on the photon energy and incident angle. The energy range of γ -ray measurements covers the incident photon energy interval from 20 keV to 20 MeV.

The instrument has two operational modes: waiting and triggered. While in the waiting mode, the count rates (lightcurve) are recorded in three energy bands (G1, G2 and G3) covering roughly 20–1,500 keV (Extended Data Table 3), with 2.944-s time resolution. When the count rate in the roughly 80–350-keV band exceeds an approximately 9σ threshold above the background on one of two fixed timescales (1 s or 140 ms), the instrument switches into the triggered mode.

In the triggered mode, lightcurves are recorded in the same bands, starting from 0.512 s before the trigger time T_0 , with time resolution varying from 2 ms to 256 ms. For the bursts of interest here, the whole time history is available with 2-ms resolution.

Multichannel spectral measurements are carried out, starting from T_0 (no multichannel spectra are available before T_0) in two overlapping energy intervals, PHA1 and PHA2 (Extended Data Table 4), with 64 spectra being recorded for each interval over a 63-channel, pseudo-logarithmic energy scale. The first four spectra are measured with a fixed accumulation time of 64 ms to study short bursts.

For this analysis, we use a standard Konus–Wind dead-time correction procedure for lightcurves (with a dead time of a few microseconds) and multichannel spectra (with a dead time of about 42 μ s).

Temporal analysis. For the temporal analysis, we used time histories from $T_0 - 0.512$ s to $T_0 + 0.512$ s in three energy bands (G1, G2 and G3), with a time resolution of 2 ms. The total burst duration T_{100} , and the T_{90} and T_{30} durations (the time intervals that contain 5%–95% and 25%–75% of the total burst count fluence, respectively⁵⁶), were calculated using the lightcurve in the roughly 80–1,500-keV energy band (G2 + G3). Burst start and end times in each band were calculated at the 5σ level using a method similar to that developed for BATSE⁵⁷. The background count rates, estimated using the data from about $T_0 - 2,500$ s to about $T_0 - 150$ s, are 958.7 s^{-1} (G1), 349.5 s^{-1} (G2) and 223.0 s^{-1} (G3) for GRB 200415A, and $1,080.3 \text{ s}^{-1}$ (G1), 394.0 s^{-1} (G2) and 135.5 s^{-1} (G3) for GRB 051103.

Spectral analysis. For the bursts of interest, we analysed multichannel and three-channel Konus–Wind energy spectra. The multichannel spectra accumulation intervals are presented in Extended Data Tables 5 and 6. The background multichannel spectra were extracted in the intervals from $T_0 + 8.448$ s to $T_0 + 491.776$ s and from $T_0 + 98.560$ s to $T_0 + 491.776$ s for GRB 200415A and GRB 051103, respectively. The emission evolution at a finer timescale can be explored using three-channel spectra, constructed from the counts in the G1, G2 and G3 energy bands in the six intervals (Extended Data Tables 5, 6). Details on Konus–Wind three-channel spectral analysis can be found elsewhere¹⁸.

We performed the spectral analysis in XSPEC, version 12.10.1⁵⁸, using the following spectral models: a simple power law, a custom exponential cutoff power-law (CPL) parameterized by the peak of νF_ν spectrum and with the energy flux as the model normalization, the Band GRB function⁵⁹, a single blackbody (BB) function with the normalization proportional to the surface area, and a sum of the CPL and BB functions (CPL + BB). The details of each model are as follows: the power law model is described by

$$f_{\text{PL}} = A \left(\frac{E}{E_n} \right)^\alpha,$$

the custom exponential CPL model by

$$n(E) = \left(\frac{E}{E_n} \right)^\alpha \exp \left[-\frac{E(2+\alpha)}{E_p} \right],$$

$$f_{\text{CPL}} = \frac{Fn(E)}{\int_{E_{\text{min}}}^{E_{\text{max}}} n(E)E dE},$$

and the Band function by

$$f_{\text{Band}} = A \begin{cases} \left(\frac{E}{E_n} \right)^\alpha \exp \left[-\frac{E(2+\alpha)}{E_p} \right], & E < \frac{(\alpha-\beta)E_p}{2+\alpha}, \\ \left(\frac{E}{E_n} \right)^\beta \left[\frac{E_p(\alpha-\beta)}{E_n(2+\alpha)} \right]^{-(\alpha-\beta)} \exp(\beta-\alpha), & E \geq \frac{(\alpha-\beta)E_p}{2+\alpha}, \end{cases}$$

where $f_{\text{PL,CPL,Band}}$ is the relevant photon spectrum (measured in photons $\text{cm}^{-2} \text{ s}^{-1} \text{ keV}^{-1}$), A is the model normalization, $E_n = 100$ keV is the pivot energy, E_p is the peak energy of the νF_ν spectrum and F is the model energy flux in the $E_{\text{min}}-E_{\text{max}}$ energy band; α and β are the low-energy and high-energy photon indices, respectively, and $n(E)$ is the unnormalized photon spectrum. The single BB function is the bbodyrad XSPEC model.

The Poisson data with Gaussian background statistic (PG-stat) was used in the model-fitting process as a figure of merit to be minimized. The spectral channels were grouped to have a minimum of one count per channel to ensure the validity of the fit statistic. Because the CPL fit to a three-channel spectrum has zero degrees of freedom (and, in the case of convergence, PG-stat = 0), we do not report the statistic for such fits. The 68% confidence intervals of the parameters were calculated using the command `steppar` in XSPEC.

A summary of constrained spectral fits with the CPL, BB and CPL + BB models is presented in Extended Data Tables 5 and 6. For GRB 200415A and GRB 051103, the power-law model failed to describe the spectra, with PG-stat/dof > 10 in all cases. Use of the Band GRB function does not constrain the high-energy photon index β for GRB 200415A spectra, and only marginally improves the CPL fit to the time-integrated spectrum of GRB 051103, with similar (within errors) E_p and α , and $\beta \approx -3$.

Burst energetics. For both bursts, the total energy fluence S was derived using the 20 keV–10 MeV energy flux of the best-fitting (CPL + BB) spectral model. Because the time-integrated spectrum accumulation interval differs from the T_{100} interval, a correction that accounts for the emission outside the time-integrated spectrum was introduced when calculating S .

The peak flux F_{peak} was calculated on the 4-ms scale using the energy flux of the best fit with the CPL model to the three-channel spectrum at the peak count rate interval ($T_0 - 0.002$ s to $T_0 + 0.002$ s). The peak flux of GRB 051103 estimated here is a factor of about 2.5 lower than that reported from previous analyses of Konus–Wind and RHESSI data^{9,10}, which used wider spectral intervals and did not separate the relatively soft spectrum in the huge 4-ms spike ($E_p \approx 1.2$ MeV) and the considerably harder emission observed immediately after its falling edge ($E_p \approx 3$ MeV).

Data availability

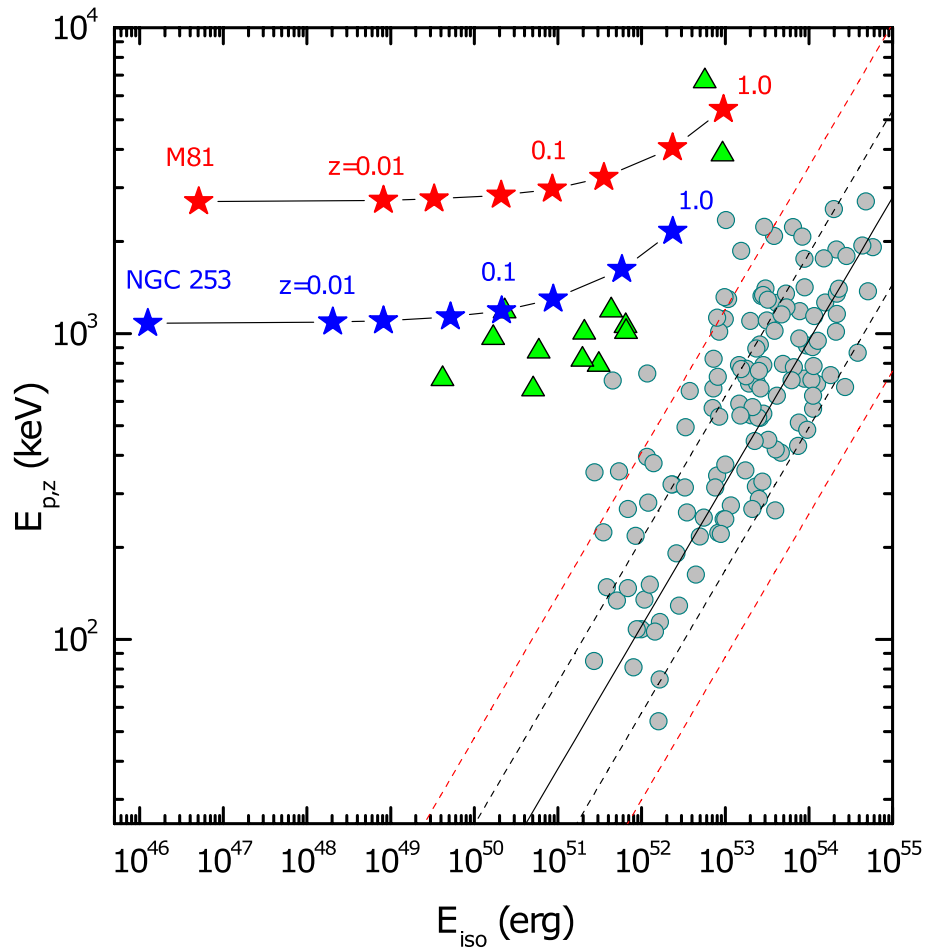
The Fermi (<https://heasarc.gsfc.nasa.gov/FTP/fermi/data/gbm/triggers/2020/bn200415367/current/>), Swift (<https://www.swift.psu.edu/guano/>) and INTEGRAL (<http://isdc.unige.ch/~savchenk/spiaccs-online/spiaccs.pl>) data are freely available online. The HEND data used for the triangulation and Konus–Wind lightcurve and spectral data are available at <http://www.ioffe.ru/LEA/papers/SvinkinNat2020/data/>. Links to the Wind ephemeris and clock accuracy data are provided in Methods. Source data are provided with this paper.

Code availability

XSPEC is freely available online (<https://heasarc.gsfc.nasa.gov/xanadu/xspec/>).

29. Meegan, C. et al. The Fermi gamma-ray burst monitor. *Astrophys. J.* **702**, 791–804 (2009).
30. Barthelmy, S. D. et al. The burst alert telescope (BAT) on the SWIFT Midex Mission. *Space Sci. Rev.* **120**, 143–164 (2005).
31. Rau, A. et al. The 1st INTEGRAL SPI-ACS gamma-ray burst catalogue. *Astron. Astrophys.* **438**, 1175–1183 (2005).
32. Ubertini, P. et al. IBIS: the imager on-board INTEGRAL. *Astron. Astrophys.* **411**, L131–L139 (2003).
33. Labanti, C. et al. The IBIS-PICsIT detector onboard INTEGRAL. *Astron. Astrophys.* **411**, L149–L152 (2003).
34. Boynton, W. V. et al. The Mars Odyssey gamma-ray spectrometer instrument suite. *Space Sci. Rev.* **110**, 37–83 (2004).
35. Hurley, K. et al. Mars Odyssey joins the third Interplanetary Network. *Astrophys. J. Suppl. Ser.* **164**, 124–129 (2006).
36. Aptekar, R. L. et al. Konus-W gamma-ray burst experiment for the GGS Wind spacecraft. *Space Sci. Rev.* **71**, 265–272 (1995).
37. Harten, R. & Clark, K. The design features of the GGS Wind and Polar spacecraft. *Space Sci. Rev.* **71**, 23–40 (1995).
38. Neubert, T. The Atmosphere-Space Interactions Monitor (ASIM) for the International Space Station. *AGU Fall Meeting Abstracts* AE42A-03 (2006).
39. The Fermi GBM Team. GRB 200415A: Fermi GBM final real-time localization. *GRB Coordinates Network* 27579 (2020).
40. Kunzweiler, F. et al. GRB 200415A: BALROG localization (Fermi Trigger 608633290 / GRB 200415367). *GRB Coordinates Network* 27580 (2020).
41. Goldstein, A. et al. Evaluation of automated Fermi GBM localizations of gamma-ray bursts. *Astrophys. J.* **895**, 40 (2020).
42. Burgess, J. M. et al. Awakening the BALROG: Bayesian location reconstruction of GRBs. *Mon. Not. R. Astron. Soc.* **476**, 1427–1444 (2018).
43. Berlato, F. et al. Improved Fermi-GBM GRB localizations using BALROG. *Astrophys. J.* **873**, 60 (2019).
44. Svinkin, D. et al. IPN triangulation of GRB 200415A (possible magnetar giant flare in Sculptor galaxy?). *GRB Coordinates Network* 27585 (2020).
45. Omodei, N. et al. GRB 200415A: Fermi-LAT detection. *GRB Coordinates Network* 27586 (2020).

46. Svinkin, D. et al. Improved IPN error box for GRB 200415A (consistent with the Sculptor galaxy). *GRB Coordinates Network* 27595 (2020).
 47. Omodei, N. et al. GRB 200415A: Fermi-LAT localization update. *GRB Coordinates Network* 27597 (2020).
 48. Lipunov, V. et al. GRB 200415A: MASTER inspection and possible localisation. *GRB Coordinates Network* 27599 (2020).
 49. Hurlley, K. et al. The Interplanetary Network. *EAS Publ. Ser.* **61**, 459–464 (2013).
 50. Hurlley, K. et al. The Interplanetary Network supplement to the Fermi GBM catalog of cosmic gamma-ray bursts. *Astrophys. J. Suppl. Ser.* **207**, 39 (2013).
 51. Pal'shin, V. D. et al. Interplanetary Network localizations of Konus short gamma-ray bursts. *Astrophys. J. Suppl. Ser.* **207**, 38 (2013).
 52. Tohuvavohu, A. et al. Gamma-ray urgent archiver for novel opportunities (GUANO): Swift/BAT event data dumps on demand to enable sensitive subthreshold GRB searches. *Astrophys. J.* **900**, 35 (2020).
 53. Hurlley, K. et al. Precise Interplanetary Network localization of the bursting pulsar GRO J1744-28. *Astrophys. J.* **537**, 953–957 (2000).
 54. Martin, D. C. et al. The Galaxy Evolution Explorer: a space ultraviolet survey mission. *Astrophys. J.* **619**, L1–L6 (2005).
 55. Gil de Paz, A. et al. The GALEX ultraviolet atlas of nearby galaxies. *Astrophys. J. Suppl. Ser.* **173**, 185–255 (2007).
 56. Kouveliotou, C. et al. Identification of two classes of gamma-ray bursts. *Astrophys. J.* **413**, L101–L104 (1993).
 57. Koshut, T. M. et al. Systematic effects on duration measurements of gamma-ray bursts. *Astrophys. J.* **463**, 570–592 (1996).
 58. Arnaud, K. A. XSPEC: the first ten years. *Astron. Soc. Pac. Conf. Ser.* **101**, 17 (1996).
 59. Band, D. et al. BATSE observations of gamma-ray burst spectra. I. Spectral diversity. *Astrophys. J.* **413**, 281–292 (1993).
- Acknowledgements** We thank E. Burns for discussions, O. Roberts for reading the manuscript and providing comments, and V. Pal'shin for contributing to the Konus-Wind and IPN data analysis tools. A.B., P.U. and J.C.R. acknowledge the continuous support from the Italian Space Agency ASI via different agreements including the latest one, 2019-35-HH.O. The Konus-Wind experiment is supported by the Russian State Space Corporation ROSCOSMOS. The HEND experiment is supported by ROSCOSMOS and implemented as part of Gamma-Ray Spectrometer suite on NASA Mars Odyssey. HEND data processing is funded by Ministry of Science and Higher Education of the Russian Federation, grant AAAA-A18-118012290370-6.
- Author contributions** D.S. and K.H. performed the IPN localization, with contributions from the Konus-Wind team (R.A., D.F., S.G., A.V.R. and T.L.C.), the Mars Odyssey (HEND and GRS) teams (I.M., D.G., A.K., M.L., A.S., W.B., C.W.F., K.P.H., H.E. and R.S.), the Fermi-GBM team (A.G., M.S.B. and C.W.-H.), the INTEGRAL (SPI-ACS and IBIS-PICsIT) teams (A.v.K., X.-L.Z., A.R., V.S., E.B., C.F., P.U., A.B. and J.C.R.), and the Swift-BAT team (S.B., J.C., H.K. and D.M.P.). D.F. and D.S. performed the Konus-Wind temporal and spectral data analysis, with contributions from A.L., A.V.R., A.T. and M.U. D.S. and D.F. wrote, and K.H. refined, the manuscript. All authors provided comments on the paper.
- Competing interests** The authors declare no competing interests.
- Additional information**
Supplementary information is available for this paper at <https://doi.org/10.1038/s41586-020-03076-9>.
- Correspondence and requests for materials** should be addressed to D.S.
- Peer review information** *Nature* thanks the anonymous reviewer(s) for their contribution to the peer review of this work. Peer reviewer reports are available.
- Reprints and permissions information** is available at <http://www.nature.com/reprints>.



Extended Data Fig. 1 | GRB 051103 (red stars) and GRB 200415A (blue stars) as possible cosmological GRBs at various redshifts ($0.01 < z < 1$). The Konus-Wind samples of short-hard GRBs and long GRBs with known redshifts²⁵ are shown by green triangles and grey circles, respectively. The recent update²⁵ for the hardness-intensity relation in the cosmological rest frame ($E_{p,z} - E_{iso}$,

'Amati' relation) is plotted as a solid line, together with its 68% and 90% prediction intervals (dashed black lines). Considering only its spectrum and energy fluence, GRB 200415A is consistent with the Konus-Wind sample of short GRBs if at redshift $z \approx 0.05-1$. In the case of GRB 051103, the implied short-GRB redshift is $z \approx 1$, with intrinsic $E_p \approx 5$ MeV.

Extended Data Table 1 | Summary of GRB 200415A and GRB 051103 properties

Parameter	GRB 200415A	GRB 051103
Host galaxy (distance)	NGC 253 (3.5 Mpc)	M81/M82 group (3.6 Mpc)
Temporal properties		
T_{rise} (ms)	$\lesssim 2$	$\lesssim 4$
τ_{cr} (ms)	~ 50	~ 50
τ_{flux} (ms)	~ 30	~ 30
T_{100} (s)	0.138	0.324
T_{90} (s)	0.100 ± 0.014	0.138 ± 0.020
T_{50} (s)	0.048 ± 0.005	0.058 ± 0.004
Peak spectrum T_0 (-0.002 s, +0.002 s), CPL model		
CPL photon index α	$-0.59^{+0.17}_{-0.17}$	$-0.13^{+0.18}_{-0.17}$
CPL Peak energy E_p (keV)	1190^{+460}_{-240}	1250^{+590}_{-290}
Time-integrated spectrum T_0 (0, +0.192 s), CPL+BB model		
CPL photon index α	$-0.02^{+0.38}_{-0.25}$	$0.08^{+0.28}_{-0.19}$
CPL Peak energy E_p (keV)	1080^{+210}_{-150}	2690^{+210}_{-180}
Blackbody temperature kT (keV)	99^{+37}_{-33}	107^{+11}_{-10}
Blackbody radius R (km)	23^{+16}_{-9} (@3.5 Mpc)	37^{+6}_{-6} (@3.6 Mpc)
Blackbody contribution to flux	$\sim 14\%$	$\sim 9\%$
Peak energy fluxes ($\text{erg cm}^{-2} \text{ s}^{-1}$), in the 20 keV–10 MeV band		
4 ms scale, T_0 (-0.002 s, +0.002 s)	$9.6^{+3.2}_{-1.6} \times 10^{-4}$	$11.5^{+5.2}_{-2.4} \times 10^{-4}$
16 ms scale, T_0 (-0.002 s, +0.014 s)	$1.11^{+0.21}_{-0.14} \times 10^{-4}$	$8.98^{+5.79}_{-2.36} \times 10^{-4}$
64 ms scale, T_0 (-0.002 s, +0.062 s)	$0.43^{+0.07}_{-0.05} \times 10^{-4}$	$4.38^{+1.61}_{-0.88} \times 10^{-4}$
Energy fluences (erg cm^{-2}), in the 20 keV–10 MeV band		
Initial spike	$3.86^{+1.27}_{-0.66} \times 10^{-6}$	$4.61^{+2.09}_{-0.96} \times 10^{-6}$
	T_0 (-0.002 s, +0.002 s)	T_0 (-0.002 s, +0.002 s)
Total	$8.5^{+1.2}_{-1.0} \times 10^{-6}$	$34.3^{+4.0}_{-2.0} \times 10^{-6}$
	T_0 (-0.004 s, +0.192 s)	T_0 (-0.006 s, +0.192 s)
Flare energetics, in the 20 keV–10 MeV band		
L_{iso} , 4 ms scale (erg s^{-1})	$\sim 1.4 \times 10^{48}$	$\sim 1.8 \times 10^{48}$
E_{iso} (erg)	$\sim 1.3 \times 10^{46}$	$\sim 5.3 \times 10^{46}$
KW maximum detection distance (Mpc)	~ 13.5	~ 15.8

Extended Data Table 2 | Triangulation annuli

Instruments involved	R.A. (J2000) (deg)	Dec.(J2000) (deg)	R (deg)	δR (deg)
GBM(0.1 ms)–KW(2 ms)	1.9406	2.0665	28.9781	0.0298
BAT(0.1 ms)–KW(2 ms)	2.0920	2.0554	28.9243	0.0262
KW(2 ms)–HEND(250 ms)	313.0127	-18.9203	54.5051	0.0394
GBM(1 ms)–HEND(250 ms)	313.3351	-18.8199	54.2444	0.0391
KW(2 ms)–PICsIT(7.8 ms)	4.1624	-2.1891	24.2751	0.1681

First column, the instruments involved in triangulation and the lightcurve temporal resolution used; second and third columns, the right ascension (R.A.) and declination (Dec.), respectively, of the centre of the annulus in the equatorial J2000 system; fourth and fifth columns, the radius of the annulus R and its half width δR , corresponding to 3σ statistical cross-correlation time delay uncertainty with systematics added in quadrature.

Article

Extended Data Table 3 | The 3σ IPN box

Box center/ vertices	R.A. (J2000) (deg)	Dec.(J2000) (deg)
Center	11.885 (00h 47m 32s)	-25.263 (-25d 15m 47s)
1	11.846 (00h 47m 23s)	-25.308 (-25d 18m 29s)
2	11.931 (00h 47m 43s)	-25.279 (-25d 16m 44s)
3	11.923 (00h 47m 42s)	-25.218 (-25d 13m 05s)
4	11.839 (00h 47m 21s)	-25.247 (-25d 14m 49s)

The area of the error box is 17 arcmin² and its maximum (minimum) dimension is 7 arcmin (4 arcmin). The Sun distance was about 37°.

Extended Data Table 4 | Konus-Wind calibrations for GRB 200415A and GRB 051103

Burst	Det.	Inc. angle (deg)	G1 (keV)	G2 (keV)	G3 (keV)	PHA1 (keV)	PHA2 (keV)
GRB 200415A	S1	62.2	22-90	90-390	390-1600	28-1600	330-20000
GRB 051103	S2	70.8	17-70	70-300	300-1200	20-1170	240-14800

Extended Data Table 5 | GRB 200415A spectral fits

Time interval (s)	Model	α	E_p (keV)	kT (keV)	R (km)	Flux (20 keV–10 MeV) (10^{-6} erg cm $^{-2}$ s $^{-1}$)	PGstat/dof
Three-channel spectra							
-0.004 – -0.002	CPL	$-0.28^{+0.58}_{-0.49}$	520^{+390}_{-140}	–	–	81^{+35}_{-17}	–
-0.002 – 0.002	CPL	$-0.59^{+0.17}_{-0.17}$	1190^{+460}_{-240}	–	–	960^{+250}_{-130}	–
0.002 – 0.032	CPL	$0.30^{+0.29}_{-0.25}$	980^{+230}_{-150}	–	–	111^{+21}_{-14}	–
0.032 – 0.064	CPL	$0.16^{+0.29}_{-0.26}$	710^{+160}_{-100}	–	–	43^{+7}_{-5}	–
0.064 – 0.096	CPL	$0.44^{+0.60}_{-0.45}$	496^{+84}_{-56}	–	–	$19.3^{+2.9}_{-2.2}$	–
0.096 – 0.128	BB	–	–	73^{+8}_{-7}	54^{+21}_{-14}	$6.8^{+1.1}_{-0.9}$	0.5/1
Multichannel spectra							
0.000 – 0.064	CPL	$0.12^{+0.15}_{-0.14}$	1066^{+91}_{-79}	–	–	$85.4^{+6.9}_{-6.3}$	55/64
0.064 – 0.128	CPL	$0.39^{+0.39}_{-0.33}$	458^{+78}_{-57}	–	–	$12.5^{+2.2}_{-1.8}$	49/47
0.128 – 0.192	BB	–	–	71^{+22}_{-15}	$26^{+12}_{-9.0}$	$1.47^{+0.57}_{-0.42}$	22/31
0.000 – 0.192	CPL	$0.01^{+0.12}_{-0.12}$	887^{+76}_{-67}	–	–	$32.3^{+2.4}_{-2.3}$	67/75
	CPL+BB	$-0.02^{+0.38}_{-0.25}$	1080^{+210}_{-150}	99^{+31}_{-32}	$23^{+16}_{-9.0}$	$33.3^{+5.1}_{-5.0}$	63/73

Extended Data Table 6 | GRB 051103 spectral fits

Time interval (s)	model	α	E_p (keV)	kT (keV)	R (km)	Flux (20 keV–10 MeV) (10^{-6} erg cm^{-2} s^{-1})	PGstat/dof
Three-channel spectra							
-0.004 – -0.002	CPL	$-0.32^{+0.43}_{-0.36}$	1380^{+9850}_{-640}	–	–	207^{+817}_{-84}	–
-0.002 – 0.002	CPL	$-0.13^{+0.18}_{-0.17}$	1250^{+590}_{-290}	–	–	1150^{+520}_{-240}	–
0.002 – 0.032	CPL	$0.20^{+0.18}_{-0.16}$	3620^{+7980}_{-1540}	–	–	940^{+1370}_{-430}	–
0.032 – 0.064	CPL	$0.64^{+0.73}_{-0.43}$	930^{+350}_{-240}	–	–	116^{+41}_{-20}	–
0.064 – 0.096	CPL	$0.28^{+0.40}_{-0.31}$	607^{+153}_{-97}	–	–	42^{+7}_{-5}	–
0.096 – 0.128	BB	–	–	93^{+8}_{-7}	47^{+7}_{-7}	$13.1^{+1.6}_{-1.5}$	0.8/1
Multichannel spectra							
0.000 – 0.064	CPL	$-0.02^{+0.08}_{-0.08}$	2570^{+160}_{-150}	–	–	444^{+27}_{-25}	93/77
	CPL+BB	$0.39^{+0.34}_{-0.24}$	2790^{+200}_{-150}	129^{+22}_{-18}	$35.5^{+8.1}_{-8.9}$	444^{+32}_{-31}	83/75
0.064 – 0.128	CPL	$0.47^{+0.25}_{-0.23}$	565^{+53}_{-45}	–	–	$34.2^{+3.1}_{-2.8}$	57/58
0.128 – 0.192	CPL	$0.66^{+1.30}_{-0.87}$	320^{+119}_{-67}	–	–	$5.5^{+1.0}_{-0.9}$	29/43
	BB	–	–	75^{+9}_{-8}	45^{+9}_{-8}	$5.1^{+0.8}_{-0.7}$	30/44
0.000 – 0.192	CPL	$-0.30^{+0.06}_{-0.06}$	2300^{+150}_{-140}	–	–	162^{+9}_{-9}	127/85
	CPL+BB	$0.08^{+0.28}_{-0.19}$	2690^{+210}_{-180}	107^{+11}_{-10}	36^{+6}_{-7}	162^{+11}_{-10}	98/83